Vietnam Journal of Mechanics, NCST of Vietnam Vol. 23, 2001, No 2 (116 – 128)

3-D NUMERICAL SIMULATION OF THE TIDAL CIRCULATION IN THE GULF OF TONKIN, VIETNAM

PHAN NGOC VINH[1], NGUYEN KIM DAN[2]
[1] *Institute of Mechanics, 264 Doican, Hanoi, Vietnam*
[2] *Laboratoire de Mecanique, Université de Caen, France*

ABSTRACT. The purpose of this paper is to present 3-D numerical simulation of the tidal circulation in the Gulf of Tonkin. A sigma-coordinate system transformation is used to make possible a total fitting between the computing point-grid and the bottom topography as well as the free water surface. A turbulence-closure sub-model K-L which permits the parameterization of the turbulence mixing is also included. The studied domain, the whole Gulf of Tonkin, extends from the coastal zone of Quang-Ninh into ThuaThienHue province and as far as Hai-Nam (China) island seawards. The model have been calibrated and verified by the observed data at six different stations for a three and seven-day periods. The results are in good agreement with the obseved data. The kinetic energy distribution was considered.

Keywords. 3-D numerical simulation, finite-difference scheme, the Gulf of Tonkin.

Introduction

The Gulf of Tonkin, one of the two largest gulfs in the South China Sea, is situated between Hai-Nam Island of China and the north coast of Vietnam. This is a rather shallow sea area with the average depth of about 45 m and the maximum one of 100 m at the mouth (Fig. 1). It is known that the tide regime is diurnal nearly in the whole gulf. The largest tide amplitude can reache 2.5 m at the head of the gulf.

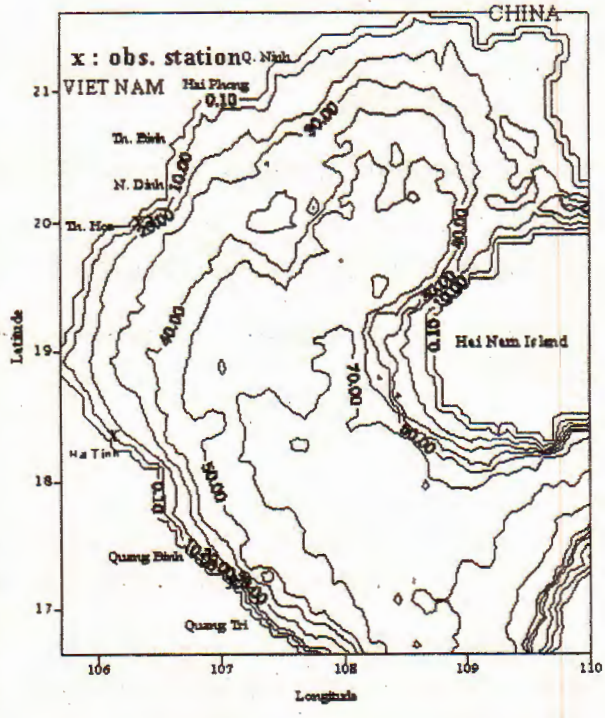

Fig. 1. Depth contours Map the Gulf of Tonkin

The aim of this paper is to present a 3-D numerical study of the tidal circulation in the Gulf of Tonkin. In the model, the Navier-Stockes equations, which are simplified by the hydrostatic approximation and by Boussinesq's one for the density distribution, have been solved with the help of a two-mode technique: the water levels are determined in the external mode and the velocity

and scalar variables are then evaluated in the internal mode. The advection terms have been handled by a characteristic method to prevent numerical oscillations and artificial diffusions (Nguyen and Martin 1988).

I. MATHEMATICAL MODEL

1. Governing equations

The governing equations are as follows:
Continuity equation:

$$\frac{\partial u}{\partial x}+\frac{\partial v}{\partial y}+\frac{\partial w}{\partial z}=0. \tag{1.1}$$

Momentum equations:

$$\frac{\partial u}{\partial t}+u\frac{\partial u}{\partial x}+v\frac{\partial u}{\partial y}+w\frac{\partial u}{\partial z}+\frac{1}{\rho}\frac{\partial P}{\partial x}=fv+\frac{\partial}{\partial z}\Big(K_M\frac{\partial u}{\partial z}\Big)+F_x, \tag{1.2}$$

$$\frac{\partial v}{\partial t}+u\frac{\partial v}{\partial x}+v\frac{\partial v}{\partial y}+w\frac{\partial v}{\partial z}+\frac{1}{\rho}\frac{\partial P}{\partial y}=-fu+\frac{\partial}{\partial z}\Big(K_M\frac{\partial v}{\partial z}\Big)+F_y, \tag{1.3}$$

$$\frac{\partial P}{\partial z}=-\rho g, \tag{1.4}$$

where, the x, y axes are horizontal and the z axis is taken positive upwards and the coordinate origin is placed at the mean water level; t is time variable; u, v, w are velocity components in the x, y and z directions, respectively; P is the pressure which can be obtained by:

$$P=P_0+\rho_0 g\eta+g\int_z^0\rho d\xi \tag{1.5}$$

where, ρ is the in-situ water density; ρ_0 is the reference water density; g is the acceleration of gravity; f is the Coriolis parameter, defined as $f=2\Omega\sin\phi$, where Ω is the angular frequency of earth rotation and ϕ is latitude of the studied location; K_M is the vertical turbulent viscosity coefficient; F_x, F_y are the horizontal diffusivities, which are defined as follows:

$$F_x=A_M\Big(2\frac{\partial^2 u}{\partial x^2}+\frac{\partial}{\partial y}\big(\frac{\partial u}{\partial y}+\frac{\partial v}{\partial x}\big)\Big);\quad F_y=A_M\Big(2\frac{\partial^2 v}{\partial y^2}+\frac{\partial}{\partial x}\big(\frac{\partial u}{\partial y}+\frac{\partial v}{\partial x}\big)\Big), \tag{1.6}$$

where, A_M is the horizontal turbulent diffusivity, which is assumed constant in the present study.

2. Initial conditions

At the initial time $t=0$, velocity components of u, v, w, surface water level η and other variables are given.

3. Boundary conditions

- At the water surface:

$$\rho K_M\Big(\frac{\partial u}{\partial z},\frac{\partial v}{\partial z}\Big)=(\tau_{sx},\tau_{sy}),\quad w_s=u_s\frac{\partial \eta}{\partial x}+v_s\frac{\partial \eta}{\partial y}+\frac{\partial \eta}{\partial t}\cdot \tag{3.1}$$

- At the bottom:

$$\rho K_M\Big(\frac{\partial u}{\partial z},\frac{\partial v}{\partial z}\Big)=(\tau_{bx},\tau_{by}),\quad w_b=-\Big(u_b\frac{\partial h}{\partial x}+v_b\frac{\partial h}{\partial y}\Big), \tag{3.2}$$

where, u_s, v_s, w_s are velocity components at the water surface; u_b, v_b, w_b are velocity components at the bottom; (τ_{sx},τ_{sy}) is wind stress at the water surface and (τ_{bx},τ_{by}) is bed shear stress; η is the water surface elevation; h is the bottom depth.

- At the land boundary: The velocity components normal to walls are null, i.e. $U_n=0$. In addition, for the tangential component of velocity, a no-slip condition at the wall is used.

- At the open boundary: Commonly, at the open boundaries, tide surface elevation is a priori prescribed as Dirichlet's conditions at all times.

4. Turbulent closure sub-model K-L

The governing equations contain the parameterized Reynolds stress and the flux terms, which take into account the turbulent diffusion of momentum, salt. The parameterization of turbulence in the model described here is based on the work of Li et al. (1997). This is an one equation sub-model, in which the turbulence kinetic energy, k has been determined from a transport equation as follows:

$$\begin{aligned}\frac{\partial k}{\partial t}+u\frac{\partial k}{\partial x}+v\frac{\partial k}{\partial y}+w\frac{\partial k}{\partial z}&=2K_M\Big[\Big(\frac{\partial u}{\partial z}\Big)^2+\Big(\frac{\partial v}{\partial z}\Big)^2\Big]\\&\quad+\frac{\partial}{\partial z}\Big(K_M\frac{\partial k}{\partial z}\Big)+\frac{2gK_{zs}}{\rho_0}\frac{\partial \rho}{\partial z}-\varepsilon+F_k\end{aligned} \tag{4.1}$$

with $F_k=\dfrac{\partial}{\partial x}\Big(A_H\dfrac{\partial k}{\partial x}\Big)+\dfrac{\partial}{\partial y}\Big(A_H\dfrac{\partial k}{\partial y}\Big)$ and the turbulent mixing length, L has been computed from the following equations proposed by Nihoul et al. (1989):

$$\varepsilon\approx\alpha_k\frac{k^2}{16K_M},\quad \alpha_k\approx 1.0, \tag{4.2}$$

$$\text{with}\quad K_M=\frac{1}{2}\alpha_k^{1/4}\sqrt{k}\,L_m;\quad L_m=(1-R_f)L_{m0}(z),$$

here, $L_{m0}(z)$ is the mixing length in the neutral case. We used the formula proposed by Escudier (1966):

$$L_{m0}(z)=\min\big[K\alpha(\eta-z_f),K(z-z_f),K(\eta-z)\big], \tag{4.3}$$

where z_f is the bottom elevation, K is the Karman constant (= 0.4) and α is a coefficient (= 0.19). R_f is the flux Richardson number:

$$R_f = -\frac{K_{zs} g \frac{\partial \rho}{\partial z}}{K_M \rho_0 \left[\left(\frac{\partial u}{\partial z} \right)^2 + \left(\frac{\partial v}{\partial z} \right)^2 \right]}. \tag{4.4}$$

The boundary conditions for equation (4.1) are (Galperin and Mellor 1990):

$$k\big|_{z=\eta} = B^{2/3} u_w^2, \quad k\big|_{z=-h} = B^{2/3} u_*^2, \tag{4.5}$$

with B is an empirical constant and taken as 16.1, u_w is the wind velocity and u_* is friction velocity at the bottom: $u_* = (\tau_b/\rho)^{1/2}$, τ_b is the friction stress.

At the open boundaries, the energy flux is considered equal to zero:

$$\left(\frac{\partial k}{\partial x}, \frac{\partial k}{\partial y} \right) = 0.$$

At the land boundaries: $k\big|_{land} = u_*^2/\sqrt{C_\mu}$; C_μ is a constant (= 0.09), (Rodi, 1980).

K_{zs} is defined from K_M (Nihoul et al, 1989): $K_{zs} = \gamma_s \sqrt{1 - R_f} K_M$; γ_s is constant (= 1.1).

5. Vertical coordinate transformation

It is desirable to introduce a non-dimensional vertical coordinate, which transforms both the surface and the bottom into the coordinate surfaces. The relationship between the old coordinate system and the new one is (Blumberg A. F. and G. L. Mellor, 1987):

$$x^* = x, \quad y^* = y, \quad \sigma = \frac{z - \eta}{h + \eta}, \quad t^* = t, \tag{5.1}$$

where, σ ranges from 0 at $z = \eta$ to -1 at $z = -h$; $H = h + \eta$ is the flow depth.

The derivative of an arbitrary variable G in the old system can be determined from the following relationships:

$$\begin{aligned}
\frac{\partial G}{\partial x} &= \frac{\partial G}{\partial x^*} - \frac{\partial G}{\partial \sigma} A_X \\
\frac{\partial G}{\partial y} &= \frac{\partial G}{\partial y^*} - \frac{\partial G}{\partial \sigma} A_Y \\
\frac{\partial G}{\partial z} &= \frac{1}{H} \frac{\partial G}{\partial \sigma} \\
\frac{\partial G}{\partial t} &= \frac{\partial G}{\partial t^*} - \frac{\partial G}{\partial \sigma} A_T
\end{aligned} \tag{5.2}$$

where,

$$A_X = \frac{\sigma}{H}\frac{\partial H}{\partial x^*} + \frac{1}{H}\frac{\partial \eta}{\partial x^*}, \quad A_Y = \frac{\sigma}{H}\frac{\partial H}{\partial y^*} + \frac{1}{H}\frac{\partial \eta}{\partial y^*}, \quad A_T = \frac{\sigma}{H}\frac{\partial H}{\partial t^*} + \frac{1}{H}\frac{\partial \eta}{\partial t^*}.$$

A new vertical velocity can now be defined as: $\omega = w - uA_X H - vA_Y H - A_T H$, which transforms the boundary condition (1.6) and (1.7) into $\omega = 0$ at $\sigma = 0$ and $\sigma = -1$.

Equations (1.1)÷(1.3) and (4.1) may now be written as (all asterisks will be dropped for notational convenience)

$$\frac{\partial \eta}{\partial t} + \frac{\partial uH}{\partial x} + \frac{\partial vH}{\partial y} + \frac{\partial \omega}{\partial \sigma} = 0, \tag{5.4}$$

$$\frac{\partial uH}{\partial t} + \frac{\partial u^2 H}{\partial x} + \frac{\partial uvH}{\partial y} + \frac{\partial u\omega}{\partial \sigma} + gH\frac{\partial \eta}{\partial x} = -fvH + \frac{\partial}{\partial \sigma}\Big(\frac{K_M}{H}\frac{\partial u}{\partial \sigma}\Big) - \frac{gH^2}{\rho}\frac{\partial}{\partial x}\int_\sigma^0 \rho d\sigma + \frac{gH}{\rho}\frac{\partial H}{\partial x}\int_\sigma^0 \sigma\frac{\partial \rho}{\partial \sigma}d\sigma + HF_x, \tag{5.5}$$

$$\frac{\partial vH}{\partial t} + \frac{\partial uvH}{\partial x} + \frac{\partial v^2 H}{\partial y} + \frac{\partial v\omega}{\partial \sigma} + gH\frac{\partial \eta}{\partial y} = fuH + \frac{\partial}{\partial \sigma}\Big(\frac{K_M}{H}\frac{\partial v}{\partial \sigma}\Big) - \frac{gH^2}{\rho}\frac{\partial}{\partial y}\int_\sigma^0 \rho d\sigma + \frac{gH}{\rho}\frac{\partial H}{\partial y}\int_\sigma^0 \sigma\frac{\partial \rho}{\partial \sigma}d\sigma + HF_y, \tag{5.6}$$

$$\frac{\partial Hk}{\partial t} + \frac{\partial uHk}{\partial x} + \frac{\partial vHk}{\partial y} + \frac{\partial \omega k}{\partial \sigma} = \frac{2K_M}{H}\Big[\Big(\frac{\partial u}{\partial \sigma}\Big)^2 + \Big(\frac{\partial v}{\partial \sigma}\Big)^2\Big] + \frac{\partial}{\partial \sigma}\Big(\frac{K_{zk}}{H}\frac{\partial k}{\partial \sigma}\Big) + \frac{2gK_{zs}}{\rho_0}\frac{\partial \rho}{\partial \sigma} - H\varepsilon + HF_k, \tag{5.7}$$

where, the horizontal viscosity and diffusion terms are defined as:

$$\begin{aligned} HF_x &= \frac{\partial \tau_{xx}}{\partial x} - \frac{\partial}{\partial \sigma}(A_X\tau_{xx}) + \frac{\partial \tau_{yx}}{\partial y} - \frac{\partial}{\partial \sigma}(A_Y\tau_{yx}) \\ HF_y &= \frac{\partial \tau_{yy}}{\partial y} - \frac{\partial}{\partial \sigma}(A_Y\tau_{yy}) + \frac{\partial \tau_{xy}}{\partial x} - \frac{\partial}{\partial \sigma}(A_X\tau_{xy}) \\ HF_k &= \frac{\partial q_x}{\partial x} - \frac{\partial}{\partial \sigma}(A_X q_x) + \frac{\partial q_y}{\partial y} - \frac{\partial}{\partial \sigma}(A_Y q_y), \end{aligned} \tag{5.8}$$

with

$$\tau_{xx} = 2A_M\Big[\frac{\partial uH}{\partial x} - \frac{\partial}{\partial \sigma}(A_X uH)\Big]; \quad \tau_{yy} = 2A_M\Big[\frac{\partial vH}{\partial y} - \frac{\partial}{\partial \sigma}(A_Y vH)\Big]$$

$$\tau_{xy} = \tau_{yx} = A_M\Big[\frac{\partial uH}{\partial y} - \frac{\partial}{\partial \sigma}(A_Y uH) + A_M\Big[\frac{\partial vH}{\partial x} - \frac{\partial}{\partial \sigma}(A_X vH)\Big]$$

$$q_x = A_H\Big[\frac{\partial Hk}{\partial x} - \frac{\partial}{\partial \sigma}(A_X Hk)\Big]; \quad q_y = A_H\Big[\frac{\partial Hk}{\partial y} - \frac{\partial}{\partial \sigma}(A_Y Hk)\Big].$$

6. Mode splitting Technique

It is desirable in terms of computer economy to seperate out vertically integrated governing equations (external mode) from the full vertical equations (internal mode). Thus, the governing equations have been solved by a two-successive-mode technique: the water-surface elevations are calculated in the external mode by a 2-D Saint-Venant equation (Nguyen and Ouahsine, 1997), and then, the scalar variables, including the components of velocity vectors, will be determined in the internal mode.

The splitting technique in terms and in directions combined with a semi-implicit finite-difference scheme proposed by Nguyen and Ouahsine (1997) is used here to solve the depth-averaged Saint-Venant equation in the external mode. In the internal mode, diffusion terms have been discretised by a finite-difference scheme, which is explicit in the horizontal x and y directions but implicit in the vertical. This is to overcome the restriction of the time steps due to numerical stabilities caused by the small vertical grid-spacings. The convections terms have been calculated by a characteristic method (see Nguyen and Martin, 1988) to prevent numerical oscillations and artificial diffusion.

II. APPLICATION

The computation domain covering the whole Gulf of Tonkin extends from $105^0$30'E to $110^0$30'E and $16^0$00'N to $21^0$45'N is discretized by a $116 \times 144 \times 10$ uniform grid. The horizontal grid spacings are 4050 m in the x-direction and in the y-direction as well. The vertical distribution of grid-points is irregular.

Six data sets observed in the field survey in 1993, 1994, 1996 and 1997 have been used to calibrate and verify the model. Amongst them, the two first data sets collected in a 3-day and a 7-day field surveys at stations: T10-LeThuy96 and T20-LeThuy96 have been used to calibrate the model. The three other data sets of a 7-day period observed at stations: T14-HaiTrieu93, T20-HaiTrieu93, T20-CuaSot94 and one data set of a 3-day period, T10-LeThuy97 have been used to verify the model. Location in longitude and latitude of the observation stations and of the periods of observation are shown in Table 1.

Calibration and verification

Several benchmarks tests (hydrostatic case and soliton case) were done to valide the mode (see [10]).

The calibration have been done by adjusting the horizontal turbulent viscosity and the Chezy coefficient. Kalkwijk (1985) estimated that: for a sea flow of mean velocity $U = 1\,\mathrm{ms}^{-1}$, and of depth $h = 50\,\mathrm{m}$, with the Chezy coefficient, $C_h = 70\,\mathrm{m}^2\mathrm{s}^{-1}$ and the horizontal turbulent viscosity is given by $A_H = 13.4\,\mathrm{m}^2\mathrm{s}^{-1}$. Values of A_H will decrease when the water depth diminishes. In the present study, as the sea depth mainly varies from 20-45 m, a uniform value of the horizontal turbulent viscosity,

$A_H = 10\,m^2s^{-1}$ is taken. Different values of the Chezy coefficient were adjusted to fit the model solution into the measured data obtained from 2 observation stations T10-LeThuy96 and T20-LeThuy96 in 1996 and the best value of C_h is $65.0\,m^2s^{-1}$. At the open boundaries, tide water level prescribed as Dirichlet's conditions at all times is determined from TIDE-FLOW2D based on the system of 2D shalow water non-linear equations.

Table 1. Location of the observation stations and the periods of observation

No.	Station	Location		Observation time
		Longitude	Latitude	
1	T10-LeThuy96	106°54'00"E	17°15'00"N	15h 31/07/96÷12h 03/08/96
2	T20-LeThuy96	106°54'35"E	17°15'08"N	06h 28/07/96÷05h 04/08/96
3	T14-HaiTrieu93	106°19'35"E	20°04'14"N	16h 15/07/93÷15h 22/07/93
4	T20-HaiTrieu93	106°21'21"E	20°02'36"N	15h 15/07/93÷14h 22/07/93
5	T20-CuaSot94	106°04'00"E	18°30'00"N	07h 22/05/94÷06h 29/05/94
6	T10-LeThuy97	106°54'00"E	17°15'00"N	08h 30/06/97÷24h 02/07/97

Figures 2a, 2b, 3a and 3b present the computed velocity values as a time series of a 3-day period from 15h 31/07/96÷12h 03/08/96 and of a 7-day period from 06h 28/07/96÷05h 04/08/96 in comparison with the observations at station T10-LeThuy96 and T20-LeThuy96. A good agreement between the computed and observed values in both amplitude and phase was obtained in the calibration case.

Five other data sets have been used for verification of the model, while preserving the model configuration obtained from the calibration step. Fig. 4a÷7b show a comparison between the computed velocity values and the observations. A good enough agreement of amplitude and phase is also again obtained in the verification case, especially at stations T14-Haitrieu93 and T20-Haitrieu93 (see Fig. 4a, 4b, 5a and 5b).

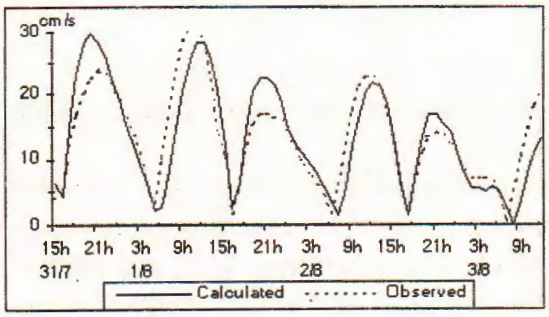

Fig. 2a. Comparison of velocity intensity at St. T10-LeThuy96, 15h 31/7-12h 3/8/96

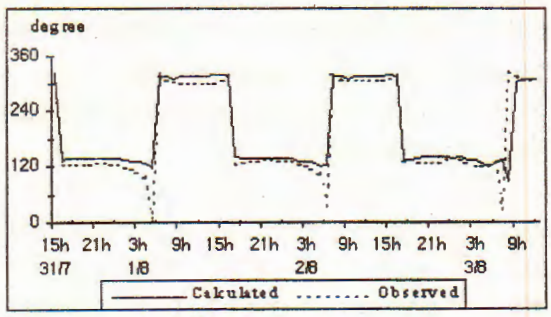

Fig. 2b. Comparison of velocity direction at St. T10-LeThuy96, 15h 31/7-12h 3/8/96

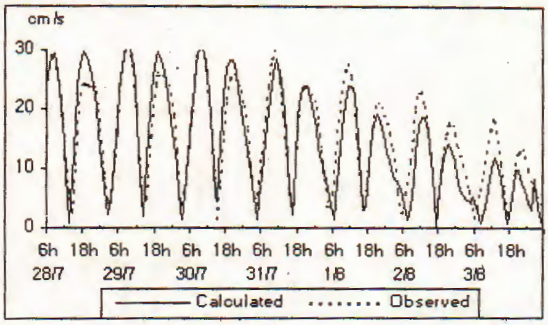

Fig. 3a. Comparison of velocity intensity at St. T20-LeThuy96, 6h 28/7-5h 4/8/96

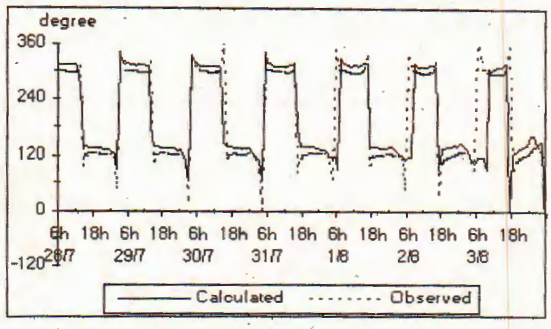

Fig. 3b. Comparison of velocity direction at St. T20-LeThuy96, 6h 28/7-5h 4/8/96

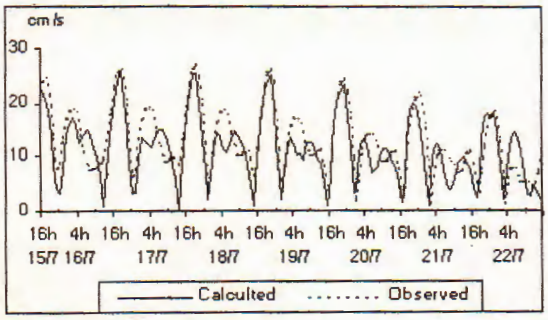

Fig. 4a. Comparison of velocity intensity at St. T14-HaiTrieu93, 16h 15/7-15h 22/7/1993

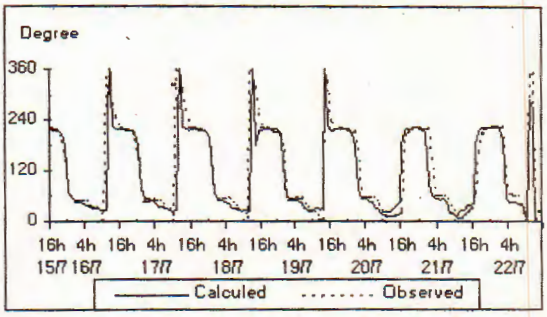

Fig. 4b. Comparison of velocity direction at St. T14-HaiTrieu93, 16h 15/7-15h 22/7/1993

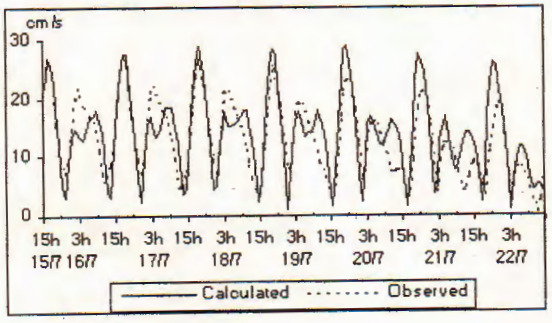

Fig. 5a. Comparison of velocity intensity at St. T20-HaiTrieu93, 15h 15/7-14h 22/7/1993

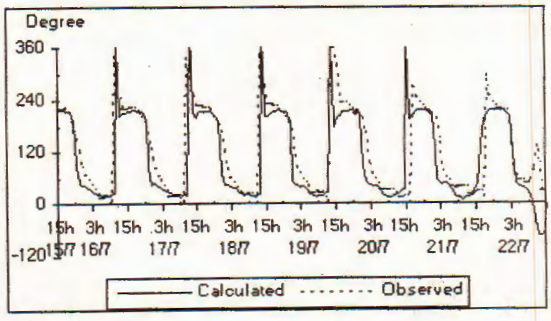

Fig. 5b. Comparison of velocity direction at St. T20-HaiTrieu93, 15h 15/7-14h 22/7/1993

Fig. 8 and 9 present the velocity fields on the surface, at the mid-depth and on the bottom at LW(Lowest water)+6 and HW(Highest water)+6, respectively. Obviously, tide currents are fairly uniform and their predominant direction is parallel to the shore line. The flow becomes stronger and more complicated near the Strait

of QuynhChau and in the South-West of the coastal zone of HaiNam island due to the irregularity of the topoporaphy.

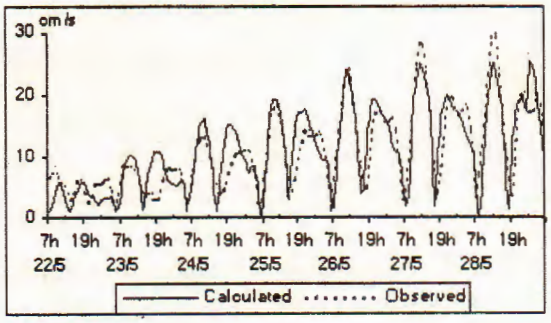

Fig. 6a. Comparison of velocity intensity at St. T20-CuaSot94, 7h 22/5-6h 29/5/1994

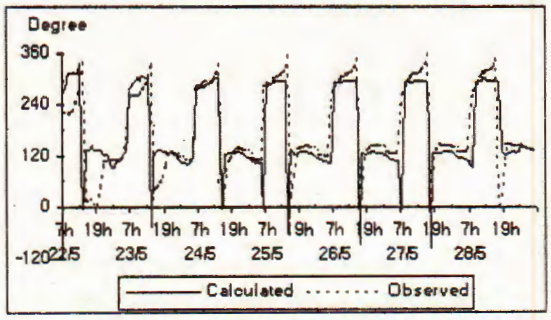

Fig. 6b. Comparison of velocity direction at St. T20-CuaSot94, 7h 22/5-6h 29/5/1994

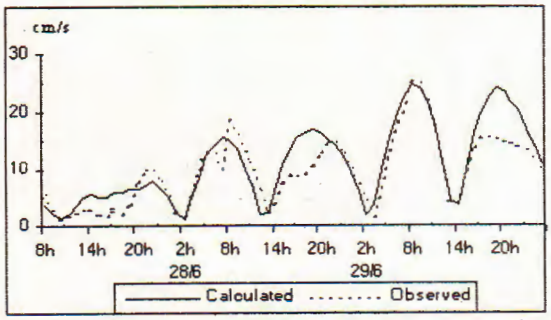

Fig. 7a. Comparison of velocity intensity at St. T10-LeThuy97, 8h 27/6-24h 30/6/97

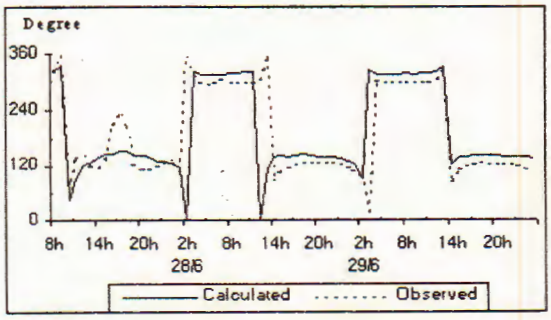

Fig. 7b. Comparison of velocity direction at St. T10-LeThuy97, 8h 27/6-24h 30/6/97

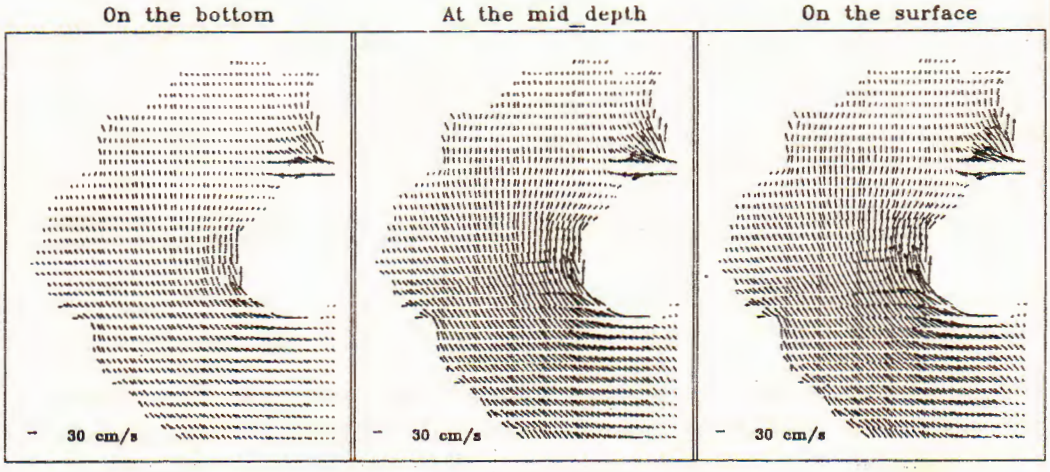

Fig. 8. Velocity field at 09h 30/7/96 (LW+6)

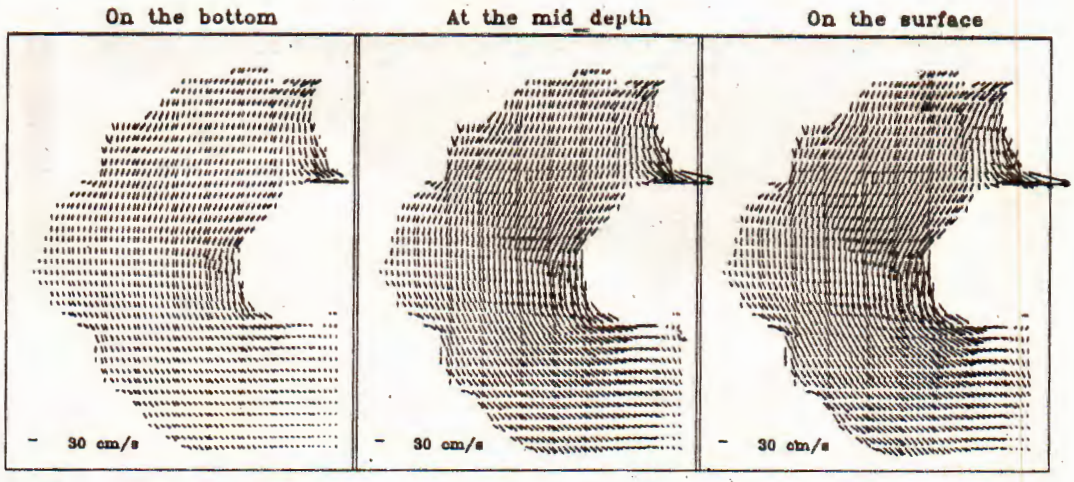

Fig. 9. Velocity field at 21h 30/7/96 (HW+6)

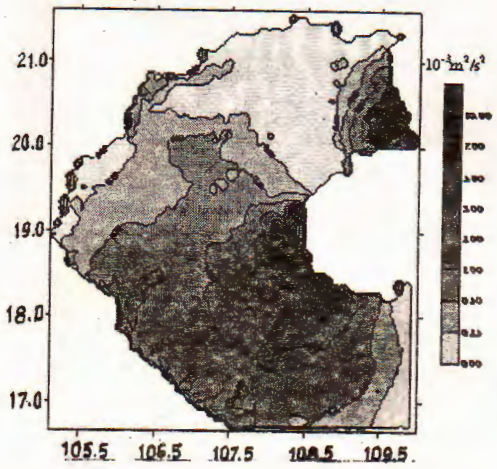

Fig. 10. Distribution of the turbulent energy on the bottom at 9h 30/7/96(LW+6)

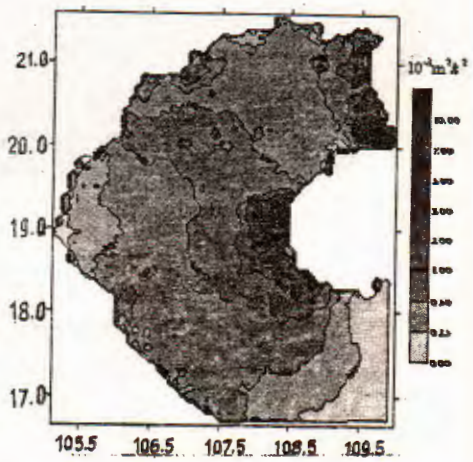

Fig. 11. Distribution of the turbulent energy on the bottom at 21h 30/7/96(LW+6)

In order to understand the hydrodynamic regime of the tidal circulation, the distribution of kinetic energy in the studied domain has been determined. Figures 10 and 11 present the contour-map of kinetic energy on the bottom at two different times: LW+6 and HW+6, respectively. We remark that the kinetic energy becomes strongest near the Strait of QuynhChau and in the South-West of the coastal zone of HaiNam island where the tide currents reach their maximum values.

Figures 12, 13, 14 and 15 show the distribution of kinetic energy together with the flow pattern on the transverse and longitudinal section at LW+6 and HW+6, respectively. Obviously, the kinetic energy is stronger near the bottom and decreases gradually to the free surface.

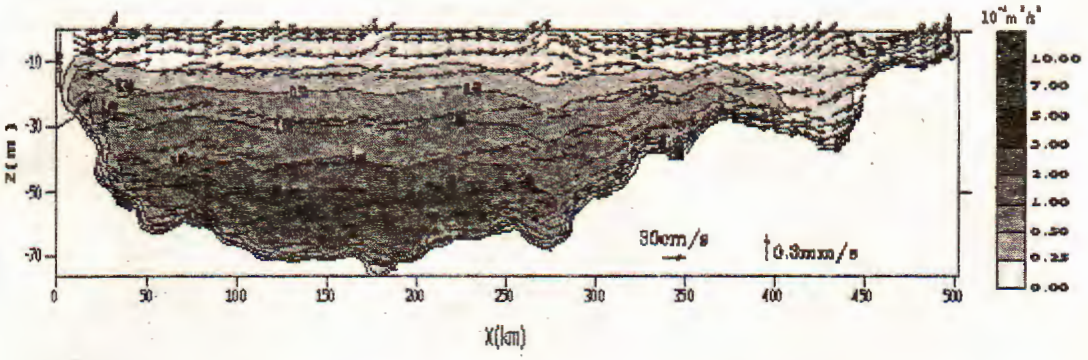

Fig. 12. Distribution of the turbulent energy & velo. field on the transverse section at 9h 10/7/96

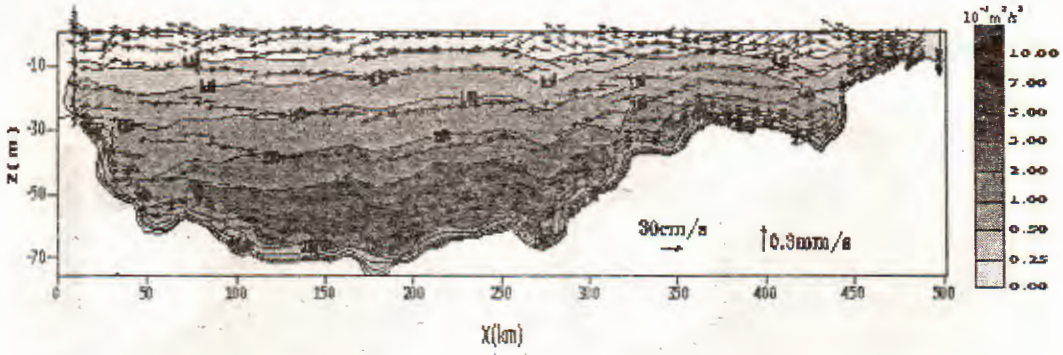

Fig. 13. Distribution of the turbulent energy & velo. field on the transverse section at 21h 30/7/96

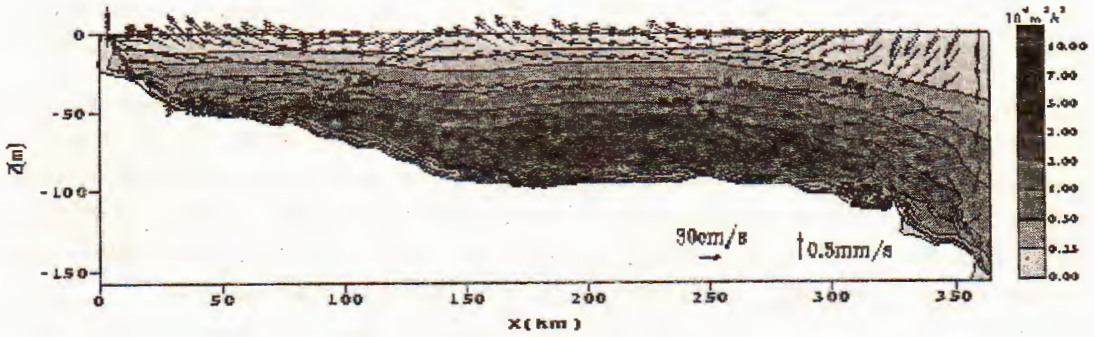

Fig. 14. Distribution of the turbulent energy & velo. field on the longitudinal section at 9h 30/7/96

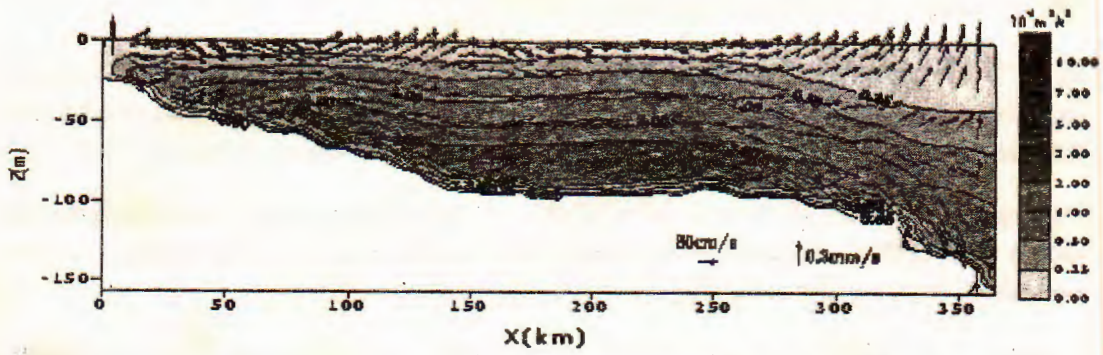

Fig. 15. Distribution of the turbulent energy & velo. field on the longitudinal section at 21h 30/7/96

Conclusions

- A numerical simulation for the tidal circulation in the Gulf of Tonkin has been performed. The model was calibrated and verified by 6 observed stations when setting the horizontal diffusivity constant and tuning the Chezy coefficient. The results show a quite good agreement between the computed results and the observations in both of the calibration and verification cases.

- A turbulence-closure sub-model K-L is applied to determine the value of the turbulent viscosity for this area.

- Generally, the predominant direction of tide currents is parallel to the shore line, the velocities range from 10-30 cms^{-1}, with a maximum one reaching around 100 cms^{-1} in QuynhChau Strait and about 50-60 cms^{-1} in the south-west of the coastal zone of Hainam island.

This work is financially supported by the Council for Natural Sciences of Vietnam.

REFERENCES

1. Blumberg A. F. and MellorG. L. (1987). Adescription of a three-dimensional coastal circulation model, in Three-dimensional Coastal Ocean Models, Coastal and Estuarinee Sciences 4, AGU, Washington D.C.,1-39.

2. Escudier M. P. (1966). The distribution of mixing length in turbulent flow near walls, Imperial College, Heat transfer Section, Report TWF/TN/1.

3. Galperin B. and Mollor G. L. (1990). A Time-dependent, Three-dimensional Model of the Delaware Bay and River System, Estuar. Coast. Shelf Sci., 31, 231-253.

4. Kalkwijk J. P. (1985). Dispersion of matter at sea under homogeneous conditions. Dt. Hydrogr., Z.38, H.6., 245-260.

5. Li Z. H., Nguyen K. D., Brun-Cottan J. C. and Martin J. M. (1994). Numerical Simulation of Saline Instrusion and Suspended Matter Transport in the Gironde Estuary by a 2-D Width-Intergrated Model, Ocenanologica Acta, 17(5):479-500.

6. Nguyen K. D. and Martin J. M. (1988). A two-dimensional fourth-order simulation for scalar trasnport in estuaries and coastal seas, J. of estuarine, Coastal and shelf Science, 20: 263-281.

7. Nguyen K. D. and Ouahsine (1997). A numerical study on the Tidal Circulation in the Strait of Dover, Journal of Waterway, Port, Coastal and Ocean Engineering, ASCE, 123 (1):8-15.

8. Nihoul J. C. J., Deleersnijder E. and Djenidi S. (1989). Modelling the general circulation of shelf seas by 3-D k-model, Earth Science Review, 26: 163-189

9. Rodi W. (1980). Turbulence models and their application in hydraulics, Monograph, International Association for Hydraulic Research, Delft, The Netherlands, 648p.

10. Establishment and use of 3D-flow programs, Report of institute of Mechanics, Hanoi (1998).

Received February 12, 2001

MÔ PHỎNG SỐ TRỊ DÒNG CHẢY THỦY TRIỀU 3 CHIỀU Ở VỊNH BẮC BỘ, VIỆT NAM

Bài báo trình bày kết quả mô phỏng số dòng chảy thủy triều 3 chiều ở Vịnh Bắc Bộ. Phép biến đổi tọa độ Sigma đã được dùng để có được sự trùng khớp giữa các điểm lưới tính và địa hình đáy cũng như là mặt thoáng. Mô hình đóng kín rối K-L cho phép tham số hóa xáo trộn rối cũng đã được ghép nối. Miền nghiên cứu trải dài từ vùng biển Quảng Ninh đến vùng biển tỉnh Thừa Thiên Huế và ra khơi đến tận đảo Hải Nam. Đã thực hiện tính toán hiệu chỉnh và kiểm nghiệm mô hình với số liệu quan trắc kéo dài 3 và 7 ngày đêm tại 7 trạm khác nhau. Kết quả cho thấy sự phù hợp chấp nhận được. Đã xem xét phân bố động năng trong vùng tính.